View Article Online
View Journal

Dalton Transactions

An international journal of inorganic chemistry

Accepted Manuscript

This article can be cited before page numbers have been issued, to do this please use: Y. Zheng, Y. Chen, L. Wang, M. Tan, Y. Xiao, B. Gao and B. Lin, *Dalton Trans.*, 2020, DOI: 10.1039/D0DT00865F.

ROYAL SOCIETY OF CHEMISTRY

rsc.li/dalton

View Article Online
DOI: 10.1039/D0DT00865F

ARTICLE

Integrating $CuInSe_2$ Nanocrystals with Polymeric Carbon Nitride Nanorods for Photocatalytic Water Splitting

Received 00th January 20xx,
Accepted 00th January 20xx

DOI: 10.1039/x0xx00000x

Yun Zheng,[*a, b, c] Yilin Chen,[a] Lvting Wang,[a] Mingyue Tan,[a] Yingying Xiao,[a] Bifen Gao[a] and Bizhou Lin[a]

Developing photocatalysts with improved photoactivity and efficiency has remained an enduring theme both fundamentally and technologically in the field of photocatalysis. Polymeric carbon nitride (CN) has been widely exploited as an earth-abundant photocatalyst for water redox reactions. Nevertheless, the limited visible-light utilization rate and the high recombination rate of photoinduced charge carriers give rise to the moderate photocatalytic reactivity of CN in water splitting. Herein, p-type $CuInSe_2$ nanocrystals are prepared by a solvothermal approach and then immobilized with n-type CN nanorods through self-assembly and thermal treatment process, forming a $CuInSe_2$/CN hybrid photocatalyst. Benefiting from the p-n heterojunction, 3% $CuInSe_2$/CN nanocomposite photocatalyst exhibits a three-fold increase in the hydrogen evolution rate (HER) than that of bare CN nanorods owing to the strengthened visible-light capturing capability and improved separation rate of photoexcited charge carriers. This work paves new avenues for the construction of p-n heterojunction photocatalysts for solar fuel production.

1. Introduction

Heterogeneous photocatalysis, which is recognized as a feasibility approach for resolving energy and environmental problems, has stimulated great research interest in the past 40 years.[1] Photocatalytic water splitting has drawn great attention attributed to its potential to produce hydrogen fuels by exploiting renewable solar energy. The creation of photocatalysts with superior photocatalytic performance remains to be the major task of photocatalytic water splitting.[2]

In the past decades, polymeric carbon nitride (CN) has been widely developed and utilized as a promising photocatalyst for water splitting and other photoredox reactions owing to the advantages of visible-light absorption, stability, sustainability and low preparation cost.[3] Nevertheless, the photocatalytic reactivity of pristine CN is relatively moderate owing to the limited utilization rate of the solar spectrum and serious recombination of photoexcited charge carriers.[4] Nanostructure engineering is one of the efficient pathways to overcoming such impediments of CN.[5] Our group demonstrated that CN nanorods could serve as an effective photocatalyst for water splitting because the nanorod structure could facilitate photogenerated electron separation and offer more active sites.[6] Additionally, extensive effort has been made to further promoting the photocatalytic performance of CN by constructing heterojunction photocatalysts by coupling CN with other semiconductors.[7] Particularly, when p-type semiconductor is coupled with n-type semiconductor, the separation of photoinduced charges is efficiently improved owing to the formation of a built-in electric field across the p-n junction region.[8] Thus, the p-n junctions formed in the nanocomposite photocatalysts could efficiently promote the photocatalytic performance for water splitting and other photoredox reactions.[9]

Recently, I-III-VI_2 compounds, especially for ternary copper indium diselenide ($CuInSe_2$) nanocrystals, are recognized as promising materials for photovoltaic and photocatalytic applications owing to the high absorption coefficients, optimal band gap energy, superior radiation stability and low toxicity.[10] $CuInSe_2$ nanocrystals could be colloidally prepared at low cost to generate products of highly uniform nanoparticles with controllable size.[11] Meanwhile, the optical absorption of $CuInSe_2$ with the low bandgap of ca. 1.0 eV is located in the region of visible and near-infrared light and greatly matches the solar spectrum.[12] Furthermore, the hybridization of $CuInSe_2$ with semiconductors has been demonstrated to result in enhanced photocatalytic activity owing to the better visible-light capturing capability and higher

[a.] Fujian Key Laboratory of Photoelectric Functional Materials, College of Materials Science and Engineering, Huaqiao University, Xiamen, Fujian 361021, P. R. China. E-mail: zheng-yun@hqu.edu.cn
[b.] Institute of Luminescent Materials and Information Display, College of Materials Science and Engineering, Huaqiao University, Xiamen, 361021, P. R. China.
[c.] State Key Laboratory of Photocatalysis on Energy and Environment, College of Chemistry, Fuzhou University, Fuzhou, Fujian 350116, P. R. China

† Electronic Supplementary Information (ESI) available: [details of any supplementary information available should be included here]. See DOI: 10.1039/x0xx00000x

View Article Online
DOI: 10.1039/D0DT00865F

charge separation efficiency owing to the formation of heterojunction.[13]

Herein, we report on the synthesis, properties, and photocatalytic reactivities of $CuInSe_2$/CN hybrid photocatalysts. The $CuInSe_2$ nanocrystals are prepared by a solvothermal approach and then coupled with CN nanorods by self-assembly and thermal treatment method to generate $CuInSe_2$/CN hybrid photocatalysts. The physicochemical properties of $CuInSe_2$/CN nanocomposites are investigated by different characterization methods, and the activities of $CuInSe_2$/CN hybrids in photocatalytic water splitting are explored.

2. Experimental

2.1. Synthesis of polymeric carbon nitride (CN) nanorods

CN nanorods were synthesized according to ref. [6]. The chiral mesoporos silica template (1 g) was dispersed and stirred in 100 mL 1 mol/L HCl solution at 80 °C for one day, followed by centrifugation and drying at 80 °C overnight. Then the silica template after acidification (0.5 g) and cyanamide (3.0 g) were mixed for 4 h in a flask connected to a vacuum line, and then sonicated at 60 oC for 4 h. Then the mixture was stirred at 60 °C for one day, and washed with H_2O, followed by centrifugation and drying at 80 °C for 12 h. Then the solids were heated at 550 °C for 4 h with a ramping rate of 2.3 °C·min^{-1} under flowing N_2. Afterward, the obtained yellow hybrids were treated with 4 mol/L NH_4HF_2 solution (**Caution!**) for 12 h to remove the silica template. After being washed with water and ethanol for several times, the solids were dried at 80 °C for 12 h under vacuum. The yield of CN nanorods is ca. 0.24 g.

2.2. Synthesis of $CuInSe_2$ nanocrystals

$CuInSe_2$ nanocrystals were synthesized according to the literature.[9a, 12a] 4 mmol CuCl, 4 mmol $InCl_3{\cdot}4H_2O$, 8 mmol Se powder, and 20 mL oleylamine were loaded in a 50 mL three-neck flask. The mixture was heated to 80 °C under an argon atmosphere with stirring for 0.5 h, vigorously stirred and quickly heated to 220 °C and incubated for 4 h, and then naturally cooled down to room temperature. Black $CuInSe_2$ nanocrystals were isolated by adding 20 mL chloroform, precipitating with 10 mL ethanol, and centrifuging at the speed of 5000 rpm for 10 min. The precipitation/centrifugation/dispersion cycle was repeated for three times. The $CuInSe_2$ nanocrystals solution was achieved by dispersing the as-obtained sediment in chloroform, while the $CuInSe_2$ nanocrystals solid was obtained by drying the suspension in an oven at 80 °C overnight.

2.3. Synthesis of $CuInSe_2$/CN hybrid photocatalyst

The appropriate amount of $CuInSe_2$ nanocrystals was mixed with 0.2 g CN nanorods powders and 10 mL chloroform. The mixture was stirred for 0.5 h, ultrasonic dispersion for 10 min and stirred with the oil bath heating at 70 °C to get the dry powders. Finally, the powders were heated at 300 °C for 30 min in the nitrogen atmosphere to obtain the $CuInSe_2$/CN hybrid. The as-prepared composite of $CuInSe_2$ nanocrystals modified CN nanorods were marked as x% $CuInSe_2$/CN. x (x= 1, 3, 5, or 10) is the mass ratio of $CuInSe_2$ to CN.

2.4. Photocatalytic hydrogen evolution

Photocatalytic hydrogen evolution arrays were performed in a Pyrex top-irradiation reaction vessel linked to a glass closed gas system. Photocatalyst powder (50 mg) was dispersed in an aqueous solution (100 mL) containing triethanolamine (10 vol.%) via sonication for 5 min. 3 wt.% Pt was loaded on the surface of photocatalyst by the in-situ photodeposition approach using $H_2PtCl_6{\cdot}6H_2O$. The suspension was evacuated for several times to remove air thoroughly before illuminated under a 300 W Xe-lamp. The wavelength of the incident light was controlled by using an appropriate long pass cut-off filter. The temperature of the reaction solution was kept at 12 ± 1 °C by a flow of cooling water. The generated gases were analyzed by gas chromatography equipped with a thermal conductive detector (TCD) with Argon as the carrier gas. Other experimental sections of synthetic procedure, characterization, are described in ESI†.

3. Results and discussion

3.1. Morphology

The surface morphologies of CN after decoration with $CuInSe_2$ were inspected by scanning emission microscope (SEM) and transmission electron microscope (TEM) techniques. SEM image of $CuInSe_2$/CN shows the uniform nanorod-like morphology with the length of ca. 1.5 μm and the outer diameter of ca. 0.2 μm (Fig. S1, ESI†). The coupling process with $CuInSe_2$ does not damage the nanorod morphology of CN (Fig. S2, ESI†). The TEM analysis indicates that small $CuInSe_2$ nanocrystals with a size of approximately 20 nm are distributed onto the surface of CN nanorods (Fig. 1, Fig. S3-S4, ESI†). The high-resolution transmission electron microscopy (HRTEM) image of $CuInSe_2$/CN showed that the $CuInSe_2$ nanoflakes are sporadic and adhered to the surface of CN nanorods compactly. The lattice fringe of d = 2.0 Å nm for (220)/(204) plane and the lattice fringe of d = 3.4 Å for (112) plane belonged to the tetragonal $CuInSe_2$ nanocrystals. C, N, Cu, In and Se elements were found in the energy-dispersive X-ray spectroscopy (EDX) spectra, verifying the successful generation of $CuInSe_2$/CN hybrids (Fig. S5, ESI†).

View Article Online
DOI: 10.1039/D0DT00865F

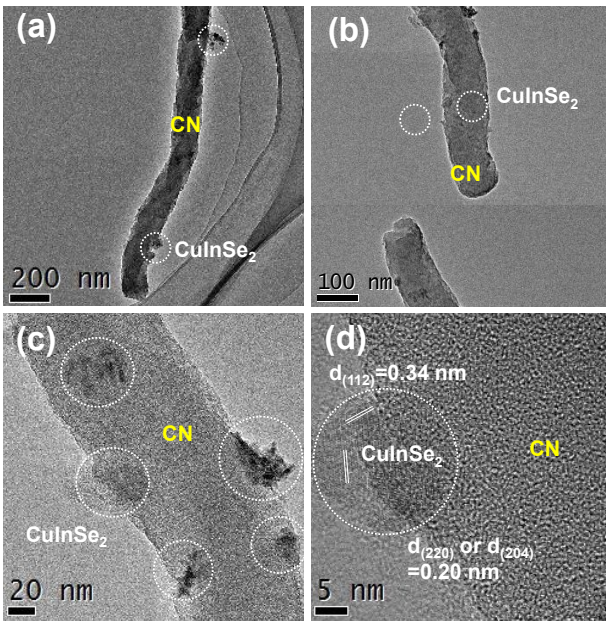

Fig. 1 (a-c) TEM and (d) HRTEM images of $CuInSe_2$/CN hybrids. The locations of $CuInSe_2$ nanocrystals are marked by white circles.

3.2. Structural characterization

X-ray diffraction (XRD) patterns were tested to reveal the chemical structure of $CuInSe_2$/CN composites. Two diffraction peaks are observed in the XRD pattern of CN nanorods, which are in good agreement with the melon-based polymeric carbon nitride reported in the previous literature.[14] The diffraction peaks at 13.0° and 27.4° correspond to (100) plane with the interplanar separation of 6.72 Å and the (002) plane with the interlayer d-spacing of 3.36 Å, respectively (Fig. 2a).[15] The diffraction peaks of the $CuInSe_2$ sample were indexed to two different phases of tetragonal and cubic $CuInSe_2$ (Fig. S6a, ESI†). The $CuInSe_2$ phase marked with '*' have been evolved into the tetragonal crystal structure (JCPDS 040-1487) with its lattice parameters a = b = 5.786 Å and c = 11.627 Å, while the phase marked with '#' have been evolved into the cubic crystal system (JCPDS 023-0208) with its lattice parameters a = b = c = 5.58 Å.[16] As shown in Table S1, EDS from fields of $CuInSe_2$ nanocrystals gave an average Cu/In/Se composition of 0.38:0.17:0.45, which is near the target 0.25:0.25:0.5 ratio, considering the error of the EDS detector (approximately 2 atom %). The XRD patterns of $CuInSe_2$/CN composites present the characteristic diffraction peaks that belonged to both CN and $CuInSe_2$, reflecting the successful hybridization of $CuInSe_2$ and CN.

The Fourier transform infrared (FT-IR) spectra of $CuInSe_2$/CN composite were presented in Fig. 2b. The peaks at 810 cm^{-1} and 1200-1600 cm^{-1} in the FT-IR spectra of CN and $CuInSe_2$/CN are indexed as the breathing mode of *s*-triazine units and the stretching mode of carbon and nitrogen heterocycles, respectively.[17] Besides, all samples possessed the broad bands in the regions of 2360 cm^{-1} and 3000-3800 cm^{-1}, originating from the physically adsorbed carbon dioxide and water in the atmosphere, respectively.

The chemical state of the $CuInSe_2$/CN hybrid was assessed by the X-ray photoelectron spectroscopy (XPS). Six major elements (C, N, O, Cu, In and Se) are examined in the XPS survey spectra of $CuInSe_2$/CN hybrid (Fig. 3). In the C 1s core level spectrum, the two peaks located at 284.8 eV and 288.0 eV correspond to sp^2 C-C bonds and sp^2-hybridized carbon in the N-containing aromatic ring (N-C=N) of CN, respectively.[18] In the N 1s core level spectrum, the two peaks centering at 398.5 eV and 400.0 eV belong to the sp^2-hybridized nitrogen in triazine rings (C-N=C) and tertiary nitrogen N-$(C)_3$ groups of heptazine heterocyclic ring units for CN, respectively. The peak at 401.2 eV corresponds to amino groups (C-N-H) owing to the incomplete polymerization of CN. Additionally, the binding energies of Cu 2p 3/2 and Cu 2p 1/2 at 954.3 eV and 935.0 eV are assigned to the oxidation state of Cu^+. The binding energies of In 3d 3/2 and In 3d 5/2 at 453.2 eV and 445.6 eV are also in good accordance with the oxidation state of In^{3+}. The binding energies of at 62.5 eV and 57.7 eV correspond to Se 3d 3/2 and Se 3d 5/2, respectively.[19] The O 1s core level at 532.9 eV (Fig. 3g) is ascribed to surface adsorbed water. No additional signal correspoding to the C–O or N–O bond is observed for the $CuInSe_2$/CN hybrid.[20] The determination of C, N, O, Cu, In and Se elements confirms the formation of $CuInSe_2$/CN hybrid.

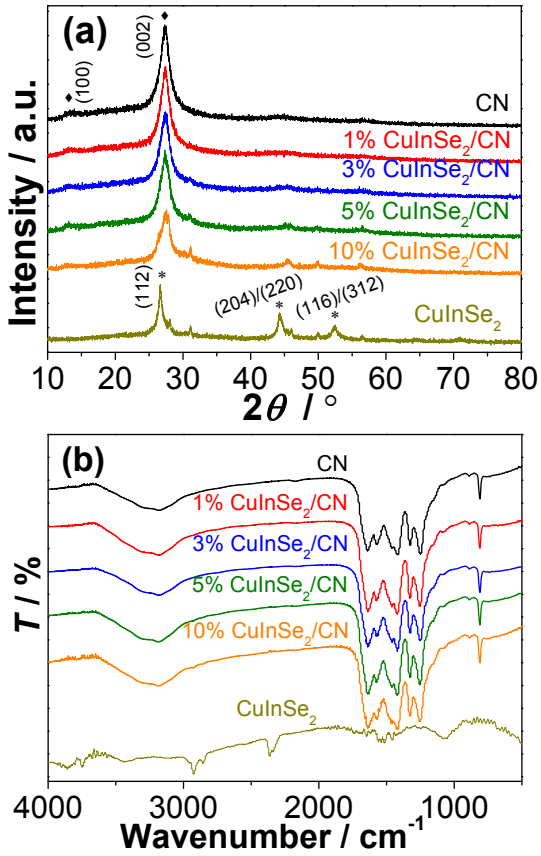

Fig. 2 (a) XRD patterns, and (b) FT-IR spectra of $CuInSe_2$/CN hybrids.

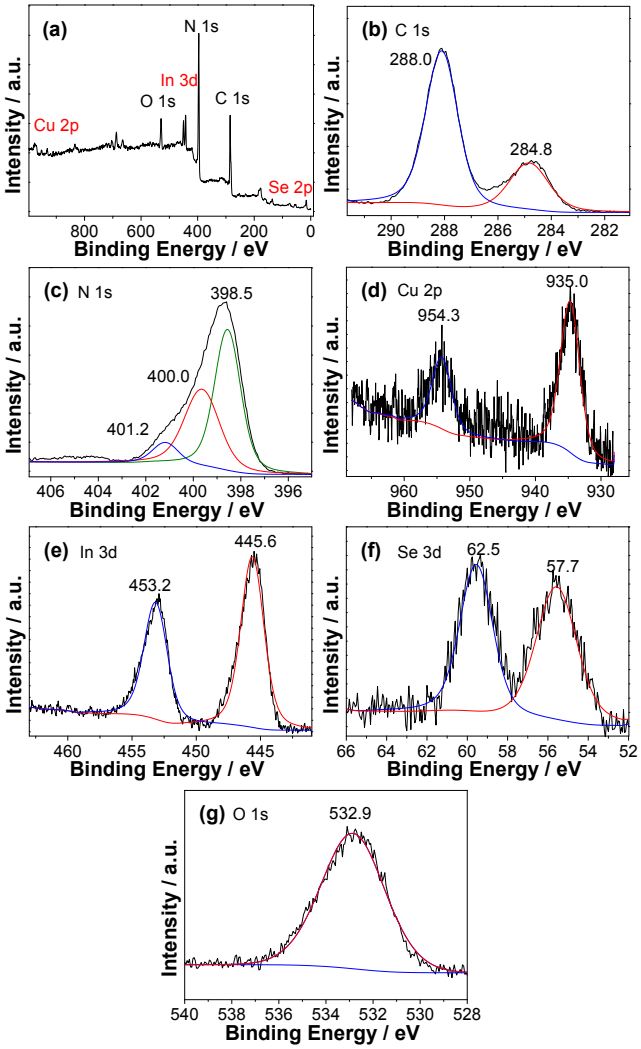

Fig. 3 (a) XPS survey, (b) C 1s, (c) N 1s, (d) Cu 2p, (e) In 3d, (f) Se 3d and (g) O 1s spectra of 3% $CuInSe_2$/CN.

3.3. Optical properties

The optical properties of $CuInSe_2$/CN were studied by ultraviolet and visible diffuse reflectance spectroscopy (UV-Vis DRS). Fig. 4a presents the UV-Vis DRS spectra of bare CN and $CuInSe_2$/CN hybrids. Pristine CN exhibits an optical absorption with an edge at 460 nm. Compared to pure CN, all the $CuInSe_2$/CN hybrids present stronger absorption capability in visible-light section ascribed to the absorption of $CuInSe_2$ (Fig. S6b-c, ESI†). As the $CuInSe_2$ content increases, the absorbance of the $CuInSe_2$/CN samples enhances gradually. These results demonstrate the greatly improved light-harvesting capability after incorporating with $CuInSe_2$, which is favorable for the optimized photocatalytic performance. The changes of light absorption ability can also be demonstrated by the color transition of the samples. The color of $CuInSe_2$/CN hybrid shifts from earthy yellow to grayish yellow with increasing $CuInSe_2$ content (Fig. S7a, ESI†).

The separation efficiency of photoinduced charge-carriers was explored by photoluminescence spectra (PL). The maximal PL intensity of pristine CN among all these samples indicates the high exciton energy of CN (Fig. 4b). The PL intensities of $CuInSe_2$/CN hybrids are much lower than that of the pristine CN due to the inhibited energy-wasteful process by introducing $CuInSe_2$ onto CN surface to construct an ideal composite system. With the increasing content of $CuInSe_2$, the PL intensities of the $CuInSe_2$/CN composites reduced gradually. According to the time-resolved photoluminescence spectra (Fig. S7b, ESI†), the average lifetime (τ_{av}) of CN and 3% $CuInSe_2$/CN composite are determined to be 1.56 ns and 1.14 ns, respectively (Table S2, ESI†). The shortened emission lifetime confirms the facilitated separation of photogenerated charge carriers of $CuInSe_2$/CN nanocomposites. Coating with $CuInSe_2$ indeed inhibits the recombination of photogenerated charge carriers.

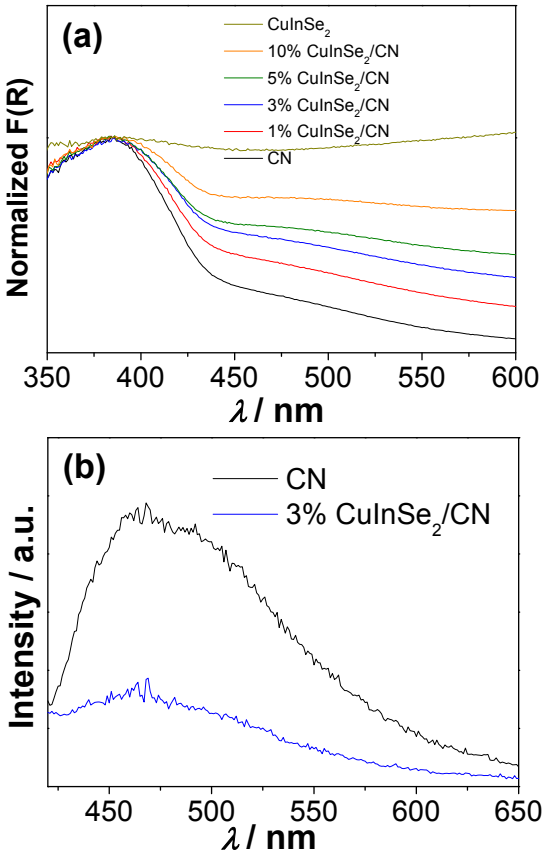

Fig. 4 (a) UV-Vis DRS spectra and (b) PL spectra of $CuInSe_2$/CN samples.

3.4. Photoelectrochemical measurements

The charge separation ability of $CuInSe_2$/CN was studied by the photo-electrochemical tests (Fig. 5). 3% $CuInSe_2$/CN sample exhibited an enhanced transient photocurrent response than pristine CN. Electrochemical impedance spectroscopy in the dark revealed that 3% $CuInSe_2$/CN shows a significantly decreased diameter in comparison with CN. These results illustrate the promoted separation of photoexcited charge carriers of $CuInSe_2$/CN hybrid.

View Article Online
DOI: 10.1039/D0DT00865F

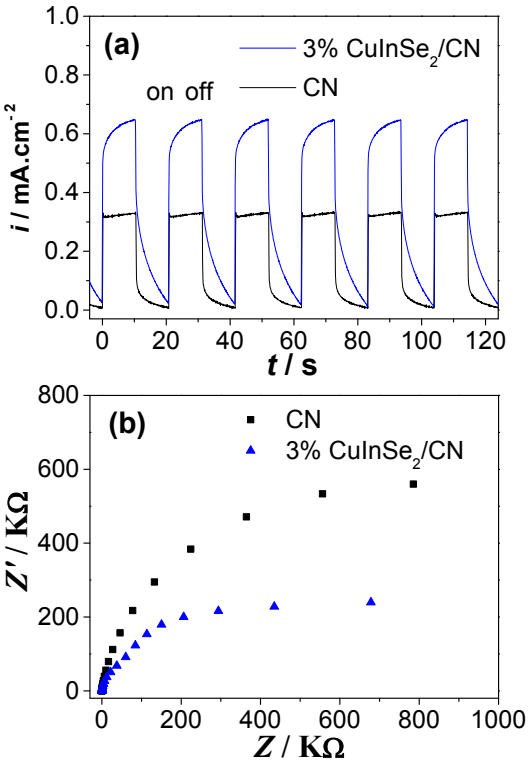

Fig. 5 (a) Periodic on/off photocurrent response, and (b) Nyquist plots of electrochemical impedance spectroscopy of $CuInSe_2$/CN samples.

3.5. Photocatalytic H_2 evolution activities

The photocatalytic reactivities of $CuInSe_2$/CN hybrids in water splitting were tested. As shown in Fig. 6a, the hydrogen evolution rate (HER) of bare CN nanorods is only 74 μmol h^{-1}. The HER of $CuInSe_2$ is negligible (0.3 μmol h^{-1}) owing to the poor dispersion of bare $CuInSe_2$ in water solution and the severe recombination of photogenerated charge carriers. The influence of $CuInSe_2$ content on the HER of $CuInSe_2$/CN hybrid photocatalysts was evaluated. The HER increases initially with the increasing $CuInSe_2$ amount and then reaches a maximum when the amount of $CuInSe_2$ loaded is about 3%. Notably, the 3% $CuInSe_2$/CN sample presents the maximum HER of 240 mol·h^{-1}, which is ca. 3 times higher than that of bare CN.

Moreover, the catalyst lifetime is also of great significance besides the photocatalytic activity. A recycling test of the photocatalytic activity of 3% $CuInSe_2$/CN hybrid was carried out (Fig. 6b). No significant variation was found in the photocatalytic activity from the first run to the fifth run. Furthermore, almost no changes were observed in the chemical structure and morphology of 3% $CuInSe_2$/CN before and after photocatalytic water splitting reactions, as demonstrated by the result of XRD, FT-IR, and SEM analysis (Fig. S8-S9, ESI†). These results confirm the good stability of $CuInSe_2$/CN hybrid in photocatalytic water splitting. Fig. 6c shows the wavelength-dependent HERs of 3% $CuInSe_2$/CN. The photocatalytic activities of 3% $CuInSe_2$/CN are in good accordance with its UV-Vis DRS spectrum, demonstrating that the water splitting reaction is driven by the captured photon for $CuInSe_2$/CN hybrid.

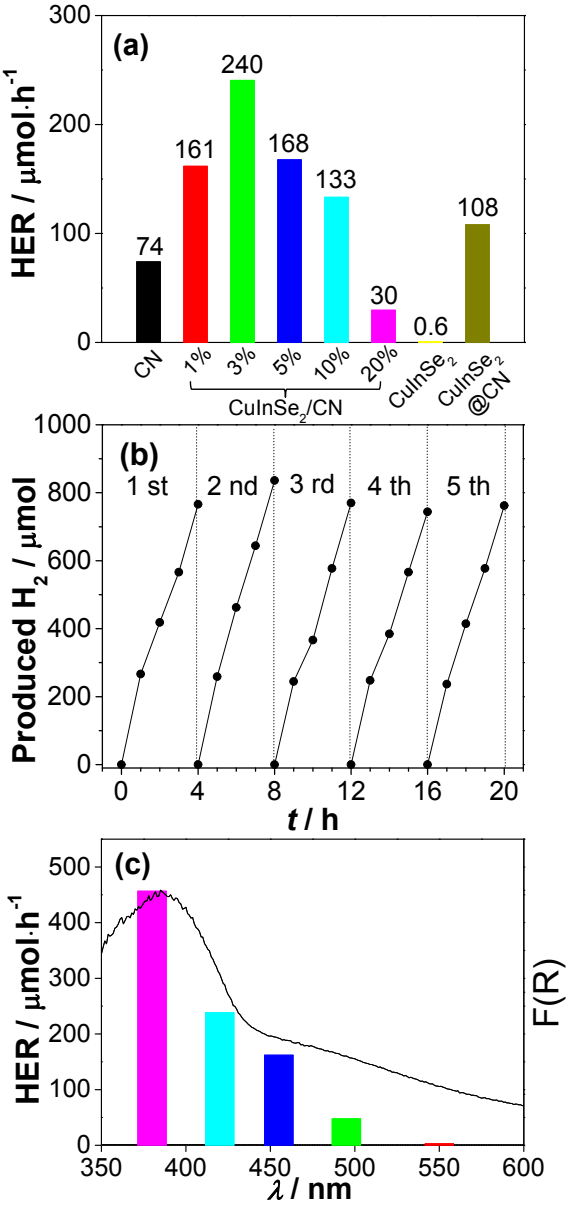

Fig. 6 (a) The HERs of $CuInSe_2$/CN samples with different amount of $CuInSe_2$, (b) Long-term water splitting test of 3% $CuInSe_2$/CN hybrid with visible light (λ>420 nm) illumination, and (c) HERs of 3% $CuInSe_2$/CN hybrid under the light irradiations with different wavelength.

3.6. Band structure and charge separation process

The energy band structures of CN and $CuInSe_2$ are investigated. As shown in the Mott-Schottky plots (Fig. S10, ESI†), the positive slope of CN corresponds to an n-type semiconductor, while a negative slope of $CuInSe_2$ corresponds to a p-type semiconductor. The flat-band potentials of CN and $CuInSe_2$ were estimated to be -0.98 and 1.11 V *vs.* RHE, which were close to the conduction band positions (E_{CB}) of CN and valence band positions (E_{VB}) of $CuInSe_2$, respectively. As shown

in Fig. S11c, a positive slope was observed for 3% $CuInSe_2$/CN, and the flat band potential was determined to be -0.93 V *vs.* RHE, which was more positive than that of CN. The optical band gaps (E_g) of 3% $CuInSe_2$/CN hybrids, CN nanorods, and $CuInSe_2$ nanocrystals were estimated from Tauc plots of $(\alpha h\nu)^2$ *vs.* photon energy ($h\nu$) (Fig. S11, ESI†). The E_g of CN nanorods, 3% $CuInSe_2$/CN hybrids, and $CuInSe_2$ nanocrystals were respectively determined to be 2.72 eV, 2.65 eV, and 1.75 eV.[16c] According to the equation: $E_{VB} = E_{CB} + E_g$, the E_{VB} of CN nanorods and 3% $CuInSe_2$/CN hybrids were calculated to be 1.74 and 1.72 V *vs.* RHE (close to the determined E_{VB} of XPS valence band spectra in Fig. S12, ESI†), and the E_{VB} of $CuInSe_2$ nanocrystals was calculated to be -0.64 V *vs.* RHE.

The energy band structures and photoinduced charge transfer pathways in the $CuInSe_2$/CN composites are put forward in Fig. 7. Both the photoinduced electron-hole pairs are generated for CN and $CuInSe_2$ with visible light illumination. When CN is in contact with $CuInSe_2$ to form a heterojunction, their Fermi energy level (E_F) reach equilibration. Meanwhile, the energy bands of CN shift downward along with the E_F, whereas the energy bands of $CuInSe_2$ shift upward along with the E_F. As a result of the built-in electric field, the electrons in the CB of $CuInSe_2$ transfer to the CB of CN, whereas the holes in the VB of CN migrate to the VB of $CuInSe_2$. The electrons accumulated on the CB of CN will transfer to the Pt nanocrystals and then initiate the H_2 evolution reaction. Since the valence band edge potential of 3% $CuInSe_2$/CN hybrid (1.72 V *vs.* RHE) and $CuInSe_2$ (1.11 V *vs.* RHE) are more positive than the redox potential of TEOA/$TEOA^+$ (0.82 V *vs.* RHE), the holes accumulated on the VB of $CuInSe_2$ can oxidize triethanolamine (TEOA).[21] Thus, the formation of p-n junctions in $CuInSe_2$/CN hybrid photocatalyst indeed inhibits the recombination of charge carriers, thus greatly benefiting the photocatalytic reactivity for water splitting.

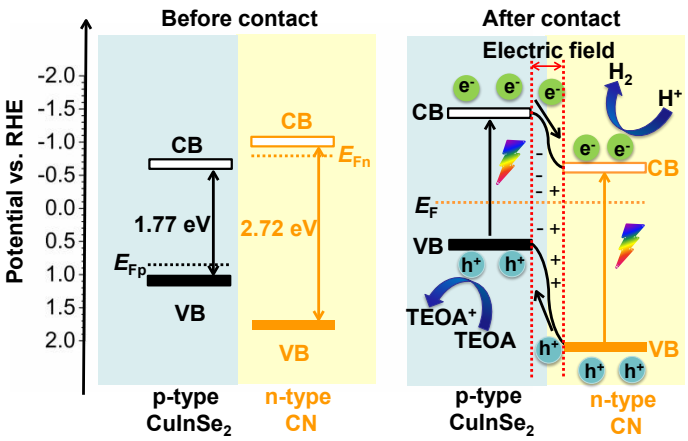

Fig. 7 Energy band structures of $CuInSe_2$ and CN before formation of the heterojunction and the band structure for $CuInSe_2$/CN heterojunction and charge separation process under illumination

4. Conclusions

View Article Online
DOI: 10.1039/D0DT00865F

In summary, n-type CN nanorods are coupled with p-type $CuInSe_2$ nanocrystals through the self-assembly and thermal treatment process to produce p-n heterojunction photocatalyst for water splitting. The $CuInSe_2$/CN nanocomposite photocatalyst exhibits greatly increased HER than the individual counterparts. The optimum hydrogen evolution rate of 3% $CuInSe_2$/CN reaches 240 $\mu mol \cdot h^{-1}$, which is 3-fold higher than that of CN nanorods. The better photocatalytic performance of the $CuInSe_2$/CN hybrid originates from the improved visible-light utilization capability and the accelerated separation of photoexcited electron-holes. This investigation paves new avenues for the construction of p-n heterojunction photocatalysts for sustainable photoredox reactions.

Conflicts of interest

There are no conflicts to declare.

Acknowledgements

The financial supports from the National Natural Science Foundation of China (21902051), the Natural Science Foundation of Fujian Province (2019J05090 and 2017J01014), the Graphene Power and Composite Research Center of Fujian Province (2017H2001), the Scientific Research Funds of Huaqiao University (605-50Y17060), and the Open Project Program of the State Key Laboratory of Photocatalysis on Energy and Environment of Fuzhou University (SKLPEE-201803) are gratefully acknowledged.

Notes and references

1 (*a*) G. Magagnano, A. Gualandi, M. Marchini, L. Mengozzi, P. Ceroni and P. G. Cozzi, *Chem. Commun.*, 2017, **53**, 1591-1594; (*b*) Y. Liu, S. Ye, H. Xie, J. Zhu, Q. Shi, N. Ta, R. Chen, Y. Gao, H. An, W. Nie, H. Jing, F. Fan and C. Li, *Adv. Mater.*, 2020, **32**, 1906513; (*c*) B. Shao, X. Liu, Z. Liu, G. Zeng, W. Zhang, Q. Liang, Y. Liu, Q. He, X. Yuan, D. Wang, S. Luo and S. Gong, *Chem. Eng. J.*, 2019, **374**, 479-493; (*d*) Y. Xu, M. Kraft and R. Xu, *Chem. Soc. Rev.*, 2016, **45**, 3039-3052; (*e*) J. Ran, X. Wang, B. Zhu and S.-Z. Qiao, *Chem. Commun.*, 2017, **53**, 9882-9885; (*f*) X. Ye, Y. Chen, C. Ling, J. Zhang, S. Meng, X. Fu, X. Wang and S. Chen, *Chem. Eng. J.* , 2018, **348**, 966-977; (*g*) S. Meng, H. Wu, Y. Cui, X. Zheng, H. Wang, S. Chen, Y. Wang and X. Fu, *Appl. Catal. B*, 2020, **266**, 118617.

2 (*a*) S. Tu, Y. Zhang, A. H. Reshak, S. Auluck, L. Ye, X. Han, T. Ma and H. Huang, *Nano Energy*, 2019, **56**, 840-850; (*b*) H. Huang, S. Tu, C. Zeng, T. Zhang, A. H. Reshak and Y. Zhang, *Angew. Chem. Int. Ed.*, 2017, **56**, 11860-11864; (*c*) A. H. Reshak, *Appl. Catal. B*, 2018, **221**, 17-26; (*d*) A. H. Reshak, *Appl. Catal. B*, 2018, **225**, 273-283; (*e*) A. H. Reshak, *J. Alloys Compd.*, 2018, **741**, 1258-1268; (*f*) H. Huang, A. H. Reshak, S. Auluck, S. Jin, N. Tian, Y. Guo and Y. Zhang, *J. Phys. Chem. C*, 2018, **122**, 2661-2672; (*g*) C. Liu, Y. Zhang, F. Dong, A. H. Reshak, L. Ye, N. Pinna, C. Zeng, T. Zhang and H. Huang, *Appl. Catal. B*, 2017, **203**, 465-474; (*h*) H. Huang, K. Xiao, T. Zhang, F. Dong and Y. Zhang, *Appl. Catal. B*, 2017, **203**, 879-888;.

3 (*a*) X. Wang, K. Maeda, A. Thomas, K. Takanabe, G. Xin, J. M. Carlsson, K. Domen and M. Antonietti, *Nat. Mater.*, 2009, **8**, 76-80; (*b*) A. Naseri, M. Samadi, A. Pourjavadi, A. Z. Moshfegh and S. Ramakrishna, *J. Mater. Chem. A*, 2017, **5**, 23406-23433.

4 (*a*) Y. Zheng, L. H. Lin, B. Wang and X. Wang, *Angew. Chem. Int. Ed.*, 2015, **53**, 12868-12884; (*b*) L. Yang, G. Dong, D. L. Jacobs, Y. Wang, L. Zang and C. Wang, *J. Catal.*, 2017, **352**, 274-281.

5 H. Ou, L. Lin, Y. Zheng, P. Yang, Y. Fang and X. Wang, *Adv. Mater.*, 2017, **29**, 1700008.

6 Y. Zheng, L. Lin, X. Ye, F. Guo and X. Wang, *Angew. Chem. Int. Ed.*, 2014, **53**, 11926-11930.

7 (*a*) W. Jiang, W. Luo, R. Zong, W. Yao, Z. Li and Y. Zhu, *Small*, 2016, **12**, 4370-4378; (*b*) Z.-D. Lei, Y.-C. Xue, W.-Q. Chen, L. Li, W.-H. Qiu, Y. Zhang and L. Tang, *Small*, 2018, **14**, 1802045; (c) L. Yang, P. Wang, J. Yin, C. Wang, G. Dong, Y. Wang and W. Ho, *Appl. Catal. B*, 2019, **250**, 42-51; (*d*) M. Zhu, S. Kim, L. Mao, M. Fujitsuka, J. Zhang, X. Wang and T. Majima, *J. Am. Chem. Soc.*, 2017, **139**, 13234-13242; (*e*) P. Qiu, C. Xu, N. Zhou, H. Chen and F. Jiang, *Appl. Catal. B*, 2018, **221**, 27-35.

8 (*a*) Y. Zheng, Y. Chen, B. Gao, J. Chen, Z. Du and B. Lin, *Mater. Lett.*, 2019, **254**, 81-84; (*b*) S. Dursun, I. C. Kaya, V. Kalem and H. Akyildiz, *Dalton Trans.*, 2018, **47**, 14662-14678; (*c*) H. Yang, Z. Jin, G. Wang, D. Liu and K. Fan, *Dalton Trans.*, 2018, **47**, 6973-6985.

9 (*a*) Z. Qin, M. Wang, R. Li and Y. Chen, *Sci. China Mater.*, 2018, **61**, 861-868; (*b*) Z. You, C. Wu, Q. Shen, Y. Yu, H. Chen, Y. Su, H. Wang, C. Wu, F. Zhang and H. Yang, *Dalton Trans.*, 2018, **47**, 7353-7361; (*c*)Y. Zhang, G. Wang, W. Ma, B. Ma and Z. Jin, *Dalton Trans.*, 2018, **47**, 11176-11189; (*d*) S. Dong, D. Wu, W. Gao, H. Hao, G. Liu and S. Yan, *Dalton Trans.*, 2020, **49**, 1300-1310.

10 (*a*) M. D. Regulacio and M.-Y. Han, *Acc. Chem. Res.*, 2016, **49**, 511-519; (*b*) A. Carlos, P. J. Sebastian and O. Solorza, *Mater. Manuf. Process*, 1997, **12**, 417-428; (*c*) L. Djellal, S. Omeiri, A. Bouguelia and M. Trari, *J. Alloys Compd.*, 2009, **476**, 584-589; (*d*) G. Liu and A. J. Bard, *J. Phys. Chem. C*, 2010, **114**, 17509-17513.

11 (*a*) S. Li, Z. Zhao, Q. Liu, L. Huang, G. Wang, D. Pan, H. Zhang and X. He, *Inorg. Chem.*, 2011, **50**, 11958-11964; (*b*) P. Sheng, W. Li, X. Tong, X. Wang and Q. Cai, *J. Mater. Chem. A*, 2014, **2**, 18974-18987; (*c*) P. Sheng, W. Li, X. Wang, X. Tong and Q. Cai, *ChemPlusChem*, 2014, **79**, 1785-1793.

12 (*a*) F. Shen, W. Que, Y. He, Y. Yuan, X. Yin and G. Wang, ACS *Appl. Mater. Interfaces*, 2012, **4**, 4087-4092; (*b*) N. Karthikeyan, T. Sivaranjani, S. Dhanavel, V. K. Gupta, V. Narayanan and A. Stephen, *J. Mol. Liq.*, 2017, **227**, 194-201; (*c*) A. Jana, K. N. Lawrence, M. B. Teunis, M. Mandal, A. Kumbhar and R. Sardar, *Chem. Mater.*, 2016, **28**, 1107-1120.

13 (*a*) Y. Liao, H. Zhang, Z. Zhong, L. Jia, F. Bai, J. Li, P. Zhong, H. Chen and J. Zhang, *ACS Appl. Mater. Interfaces*, 2013, **5**, 11022-11028; (*b*) M. Bagheri, A. R. Mahjoub and B. Mehri, *RSC Adv.*, 2014, **4**, 21757-21764; (*c*) Q. Wang, J. Qiao, J. Zhou and S. Gao, *Electrochim. Acta*, 2015, **167**, 470-475; (*d*) Z. Wu, X. Tong, P. Sheng, W. Li, X. Yin, J. Zou and Q. Cai, *Appl. Surf. Sci.*, 2015, **351**, 309-315.

14 (*a*) J. Xue, M. Fujitsuka and T. Majima, *Phys. Chem. Chem. Phys.*, 2019, **21**, 2318-2324; (*b*) D. Ruan, J. Xue, M. Fujitsuka and T. Majima, *Chem. Commun.*, 2019, **55**, 6014-6017.

15 (*a*) K. Li and W. D. Zhang, *Small*, 2018, **14**, 1703599; (*b*) Y. Chen, J. Li, Z. Hong, B. Shen, B. Lin and B. Gao, *Phys. Chem. Chem. Phys.*, 2014, **16**, 8106-8113; (*c*) H. Wang, Q. Lin, L. Yin, Y. Yang, Y. Qiu, C. Lu and H. Yang, *Small*, 2019, **15**, 1900011.

16 (*a*) Q. Guo, S. J. Kim, M. Kar, W. N. Shafarman, R. W. Birkmire, E. A. Stach, R. Agrawal and H. W. Hillhouse, *Nano Lett.*, 2008, **8**, 2982-2987; (*b*) S. Das, H. Sopha, M. Krbal, R. Zazpe, V. Podzemna, J. Prikryl and J. M. Macak, *ChemElectroChem*, 2017, **4**, 495-499; (*c*) N. Karthikeyan, T. Sivaranjani, S. Dhanavel, V. K. Gupta, V. Narayanan and A. Stephen, *J. Mol. Liq.*, 2017, **227**, 194-201.

17 Y. Zheng, Z. Yu, H. Ou, A. M. Asiri, Y. Chen and X. Wang, *Adv. Funct. Mater.*, 2018, **28**, 1705407.

18 (*a*) L. Ge, F. Zuo, J. Liu, Q. Ma, C. Wang, D. Sun, L. Bartels and P. Feng, *J. Phys. Chem. C*, 2012, **116**, 13708-13714; (*b*) D. Zheng, G. Zhang and X. Wang, *Appl. Catal. B*, 2015, **179**, 479-488; (*c*) L. Chen, Y. Xu and B. Chen, *Appl. Catal. B,* 2019, **256**, 117848.

19 C. R. Kim, S. Y. Han, C. H. Chang, T. J. Lee and S. O. Ryu, *Curr. Appl. Phys.*, 2010, **10**, S383-S386.

20 (*a*) J. Li, B. Shen, Z. Hong, B. Lin, B. Gao and Y. Chen, *Chem. Commun.*, 2012, **48**, 12017-12019; (*b*) Y. Wang, H. Wang, F. Chen, F. Cao, X. Zhao, S. Meng and Y. Cui, *Appl. Catal. B*, 2017, **206**, 417-425; (*c*) J. W. Zhang, S. Gong, N. Mahmood, L. Pan, X. Zhang and J. J. Zou, *Appl. Catal. B*, 2018, **221**, 9-16.

21 (*a*) D. Mateo, A. M. Asiri, J. Albero and H. García, *Photochem. Photobiol. Sci.*, 2018, **17**, 829-834; (*b*) C. C. Wang, Y. Q. Zhang, J. Li and P. Wang, *J. Mol. Struct.*, 2015, **1083**, 127-136; (*c*) R. J. Crutchley and A. B. P. Lever, *J. Am. Chem. Soc.*, 1980, **102**, 7128-7129.

View Article Online
DOI: 10.1039/D0DT00865F

Table of Contents Entry

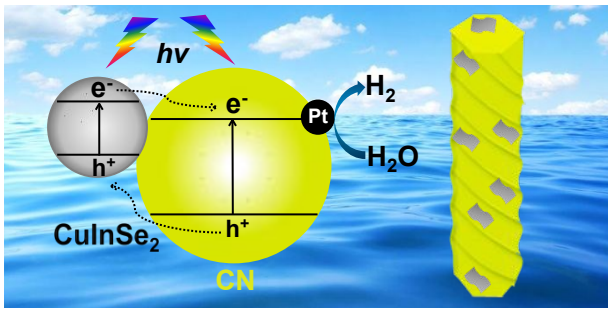

A p-n heterojunction photocatalyst for water splitting is constructed by incorporating $CuInSe_2$ nanocrystals with polymeric carbon nitride (CN) nanorods.